Received: 29/03/2021 *Accepted: 25/11/2021*

International Journal of Advances in Biomedical Engineering
Open Access Peer-reviewed Journal
ISSN: 2822-2237
www.ijabe.online
Volume:1, Number:1, Pages:(9–27)

Albumin Adsorption on a Stationary Microparticle

Mehmet Melih Tatlisoz [*1] ***and Cetin Canpolat*** [1]

**Corresponding Author E-mail: mtatlisoz@cu.edu.tr*

[1] *Department of Biomedical Engineering*
Faculty of Engineering
Cukurova University, 01250
Adana, Turkey

Abstract

In this study, the behavior of the albumin adsorption mechanism is numerically investigated within a microfluidic chip. The adsorption mechanism is modeled with the classical Langmuir approach, and electrokinetic flow conditions are employed. The spherical adsorbent surface is placed at the center of gravity of the designed microchannel. Adsorption behavior is investigated by varying the external electrical field (E), the diameter of the spherical microparticle (DP), initial protein concentration (Cinit), the existence of another solid boundary in the close proximity of the adsorbent surface, and different geometries of adsorbent surfaces, which are triangular, rhombic and square. Initially, generated numerical code is adopted to a similar experimental study, and the code validation is carried out. Adsorption behavior of the albumin varies with a consistent pattern for the inspected parameters. It is concluded that albumin adsorption can be controlled adequately with a microfluidic chip under proposed operating conditions. Moreover, many kinds of protein species can be controlled with the proposed design because of their analogical nature.

Keywords: Microfluidics; Albumin; Adsorption Phenomenon; Electrokinetics; Mathematical Modelling

1. Introduction

Protein adsorption is a significant phenomenon, especially for the topics of artificial organ failure, plaque formation, inflammation response, fouling of biomaterials, and membrane filtration units [1]. It is a standard but the complicated process [2], which depends on the electrostatic interactions between the adsorbate and the adsorbent, surface chemistry of the adsorbent, dimensions, and orientations of the proteins [3]. Biocompatibility and functionality of the biomaterials are strongly altered by the occurrence of adsorption [4]. For example, potential hazardous effects of synthetic materials can be neutralized with a biological sheath [5]. Biofluids are crowded with a wide range of protein species; hence, the protein adsorption phenomenon is frequently encountered for the foreign substances incorporated in the human body. Therefore, a significant number and highly specific research are attributed to this area, which can be listed as characterization of protein adsorption on nanoparticle surfaces [6], investigating the effect of protein corona upon the biomaterial surfaces [7], bio-compatible impacts of the protein adsorption for the metallic implants [8], the feasibility of protein adsorption for functionalizing the biomaterials [9]. Microfluidics is an emerging technology that offers great advantages, such as the requirement of meager sample amount, high resolution, high sensitivity, low costs, short analysis durations, portability [10], advanced flow, and concentration control as well as easy integration with other devices [11]. Therefore, many diverse applications are carried out with microfluidic systems, such as pathogen detection [12, 13, 14], gene delivery [15, 16] drug delivery [17, 18, 19], tissue engineering [20, 21, 22], material fabrication [23, 24, 25], food safety monitoring [26, 27] etc. Protein adsorption phenomenon is also a frequently researched field with microfluidic systems, for instance [28, 29, 30, 31]. Microfluidic platforms are mainly categorized as centrifugal, pressure-driven, capillary, acoustic, and electrokinetics based on the actuation technique [32], such that pressure-driven and electrokinetics platforms are the most frequently utilized. Electroosmosis (EO) is a type of electrokinetic technique, which is identified as the movement of an electrolyte-containing solution under the externally applied direct current (DC) or alternating current (AC) electrical field [33]. Some significant advantages are contributed to the electroosmotic-driven flow systems over the pressure-driven systems, which are plug-like flow profile characteristics, relieving from complex and expensive mechanical parts, and easier manipulation. The protein adsorption mechanism can be categorized into two classes: controlled protein adsorption and resistance to protein adsorption; the latter is referred to as antifouling [34]. For numerical modeling, protein adsorption can be modelled with three different main methods: quantum mechanics approaches, all atom empirical force field approaches, and coarse-grained approaches [35]. Quantum mechanics approaches are appropriate for the tiny species, consisting of ten atoms and extremely short time scales of 10-12 to 10-10 s. However, all-atom empirical approaches can be applied to 103 to 104 atoms, and the upper limit of the time scale is drawn to the 10-8 s. When small protein or protein fragments are modeled, all-atom empir-

ical approaches are the most suitable method. In coarse-grained approaches, the shape of the protein is assumed as a single spherical or an anisotropic particle. It can be enabled to predict the equilibrium coverages and utilizing specific boundary conditions for bulk transport equations. Moreover, a dramatic increase in the time scale of 103 to 106 s is achieved; hence, experimental situations are entirely comprised. On the contrary, predicting the adsorption behavior is diminished compared to the previous approaches. In the present study, the controllability of the protein adsorption on a spherical microparticle surface is numerically evaluated with a microfluidic chip. Fluid flow is driven by electrokinetics, and the protein species is dissolved in the fluid. An adsorbent surface is located to the center of gravity of the microchannel. No net charge density is defined for the adsorbent surface, which yields immobilization. The operating parameters of the proposed system, which are electrical field strength (E), microparticle diameter (DP), initial protein concentration (Cinit), the existence of another solid boundary in the close proximity of the adsorbent surface, and different geometries of adsorbent surfaces are systematically varied, and the obtained results are compared. Protein adsorption is modeled with the classical Langmuir approach under a coarse-grained approach. Moreover, the relevant protein is determined as human serum albumin (HSA) for which is the most abundant protein in human plasma, quantitatively 55% [36]

2. Material and Methods

2.1. Theory

Fluid is characterized as Newtonian, and flow is modeled with Navier – Stokes equation coupled with the continuity equation:

$$\rho\left(\frac{\partial u}{\partial t}+(u.\nabla)\,u\right)=-\nabla p+\mu\nabla^2 u+f \tag{1}$$

$$\nabla.u=0 \tag{2}$$

where u, ρ, p, μ, f terms are flow velocity, fluid density, fluid viscosity, pressure gradient, and body force, respectively. Bold symbols are preferred for denoting vector quantities. These equations are simplified according to the negligible compressibility nature of the liquids. However, the inertial term is not excluded because the working Reynolds number is always higher than unity, such as Re=11.17, 22.34, 33.51, 44.68, and 55.85. Adsorbate material is dissolved in the flowing fluid. Therefore, Nernst – Planck equation is employed for governing the transport of the diluted species:

$$\frac{\partial C}{\partial t}+u.\nabla C=\nabla.\left(D\nabla C+zu_mFC\nabla\varphi\right) \tag{3}$$

where C, D, z, u_m, F, φ are the concentration, diffusion coefficient, valence number, ionic mobility, Faraday constant, and electrical potential, respectively. Ionic

mobility is calculated according to Nernst – Einstein relationship, i.e., $u_m = D/RT$, where R denotes the ideal gas constant. Note that the diluted species is transported mainly by convection, which derives from electrokinetic effects. Electroosmotic fluid velocity is calculated with the Smoluchowski slip velocity equation, which is implemented as a boundary condition upon the lower and the upper walls of the microchannel:

$$u_{eo_w} = -\frac{\varepsilon \zeta_w}{\mu} E_t \tag{4}$$

where $\varepsilon, \zeta_w, E_t$ are permittivity of the fluid, the zeta potential of the microchannel wall, and the tangent of the externally applied electrical field, respectively. The externally applied electrical field is produced from the potential difference between the inlet and the outlet of the microchannel. In addition, the upper and the lower solid boundaries are electrically insulated, $n \cdot \nabla \phi = 0$. These solid boundaries are polarized concurrently, which yields the formation of an electrical double layer (EDL) adjacently. However, the existence of EDL is neglected due to possession of very low characteristic thickness, which is a few nanometers, as compared to the width of the designed microchannel. Therefore, the body force term (f) in Navier – Stokes equation is equaled to zero, and the Laplace equation is solved instead of the Poisson equation:

$$\nabla^2 \phi = 0 \tag{5}$$

Boundaries of the central adsorbent surface is also electrically insulated. However, no net charge density is determined upon the boundary; thus, zeta potential equals zero value, leading to a no-slip condition, i.e., u=0. The diluted species is adsorbed to the spherical microparticle upon the interaction. The adsorption phenomenon is occurred along with the desorption phenomenon.

$$C + B \underset{k_{des}}{\overset{k_{ads}}{\rightleftharpoons}} C_c$$

which is mathematically described with the classical Langmuir model as below:

$$\frac{\partial C_C}{\partial t} = r_{ads} - r_{des} = k_{ads} \times C \times B - k_{des} \times C_C \tag{6}$$

where C, B and C_C, k_{ads}, k_{des} are adsorbate concentration, adsorption site concentration on the surface of the adsorbent, adsorbed species concentration, adsorption rate, and desorption rate, respectively. Adsorption rate constant ($k_a ds$) and desorption rate constant (k_{des}) are held constant due to isothermal working conditions. The adsorption site concentration (B) can also be described as the subtraction between the initial surface adsorption concentration (B_0) and the instantly bounded adsorbate concentration (C_C). If this relationship is substituted in Eq. (6):

$$\frac{\partial C_C}{\partial t} = k_{ads} \times C \times (B_0 - C_C) - k_{des} \times C_C \tag{7}$$

Eq. (7) can be solved analytically for calculating complex concentration under equilibrium, which may be utilized for the purpose of code validation:

$$C_C^{eq} = \frac{k_{ads} B_0 C}{k_{ads} C + k_{des}} \tag{8}$$

The occurring adsorbate layer is always considered infinitesimally thin, which can be considered a valid approximation due to the diameters of globular proteins is a few nanometers. Adsorption reaction must be coupled with the mass transport equation due to the inclusion of a common term, which is adsorbate concentration (C). Therefore, a boundary flux condition is defined upon the functional surface of the microparticle:

$$n.(Cu - D\nabla C) = -k_{ads} \times C \times (B_0 - C_s) + k_{des} \times C_C \tag{9}$$

The microchannel domain is held empty for the adsorbate species at zero time. The adsorbate species is fed to the microchannel domain from the inlet and collected from the outlet. Lower and upper walls are defined as non-functional as well as impermeable. By this means, additional boundary conditions are introduced to the solving domain as below:

2.2. Numerical Study

In this study, the adsorption performance of an adsorbent surface is numerically investigated by systematically varying some vital parameters. 2D Simulations are performed with the commercial software of COMSOL Multiphysics 5.3a. As seen in Figure 1(a), straight rectangular microchannels are designed for $L = 1000\mu m$ and $W = 300\mu m$. A non-polarized microparticle, which holds an initial adsorption site concentration of $B_0 = 1x10 - 10mol/m^2$, is placed to the microchannel center, i.e., $H = 150\mu m$. The positive electrode with constant potential is implemented upon the left boundary, and the right boundary is grounded. Therefore, a DC electrical field is generated from left to right ends throughout the microchannel. Microparticle is determined as immobile under the electrical field by defining no net charge density. The simulation software employs finite element analysis (FEA); thus, a mesh with triangular elements is applied to the solving domain as well as a denser mesh is required at the vicinity of the adsorption-desorption reaction occurs, which is seen in Figure 1(b). A series of simulations are conducted under the same conditions with the mesh element numbers of 3256, 5600, 6614, 8120, and 11200. As a result of the mesh independence analysis, the difference between the surface adsorbate concentrations of the last couple is below 0.1%. Therefore, the mesh with 8120 elements is preferred for further simulation studies. The fluid, which incorporates adsorbate species, is introduced from the left boundary with a specific initial concentration and collected from the right boundary, as illustrated in Figure 1(c). The adsorbate species is characterized as the protein of HSA as stated in the previous section, by introducing proper values to the solving system of diffusion coefficient ($D = 2.15x10 - 11m^2/s$

[37]), adsorption rate constant ($k_{ads} = 104L/mol.s$ [38]), desorption rate constant ($k_{des} = 5.78x10^{-4}1/s$ [38]) and net charge density under physiological pH (z=-9 [39]). At the beginning of the present study, the external electrical field is varied between $100V/m \leq E \leq 500Vm$ with the step increase of $100V/m$, while the microparticle diameter is held constant for $DP = 40\mu m$. The electrical field strength is held relatively low to avoid undesired protein denaturation phenomenon, which may alter the adsorption behavior. Afterward, the diameter of the microparticle is varied between the $20\mu m \leq DP \leq 60\mu m$ with a step increase of $10\mu m$. The electrical field is determined by which the most rapid complete adsorption time. The study is maintained by investigating the adsorption effect of the initial adsorbate concentration. While the previous simulations are carried out with $C_{init} = 0.01mol/m^3$, adsorption behavior is observed with the values of $C_{init} = 0.005mol/m^3$, $C_{init} = 0.015mol/m^3$, $C_{init} = 0.02mol/m^3$, as well. The effect of the existence of another solid boundary in the close proximity of the adsorbent surface is also investigated. By this means, the microparticle is the distance between the adsorbent surface and the lower wall of the microchannel is diminished, i.e., the value $H = 10\mu m$. Finally, the spherical geometry of the adsorbent surface is altered. The adsorption performance of the triangular, rhombic, and square adsorbent surfaces is observed, as well.

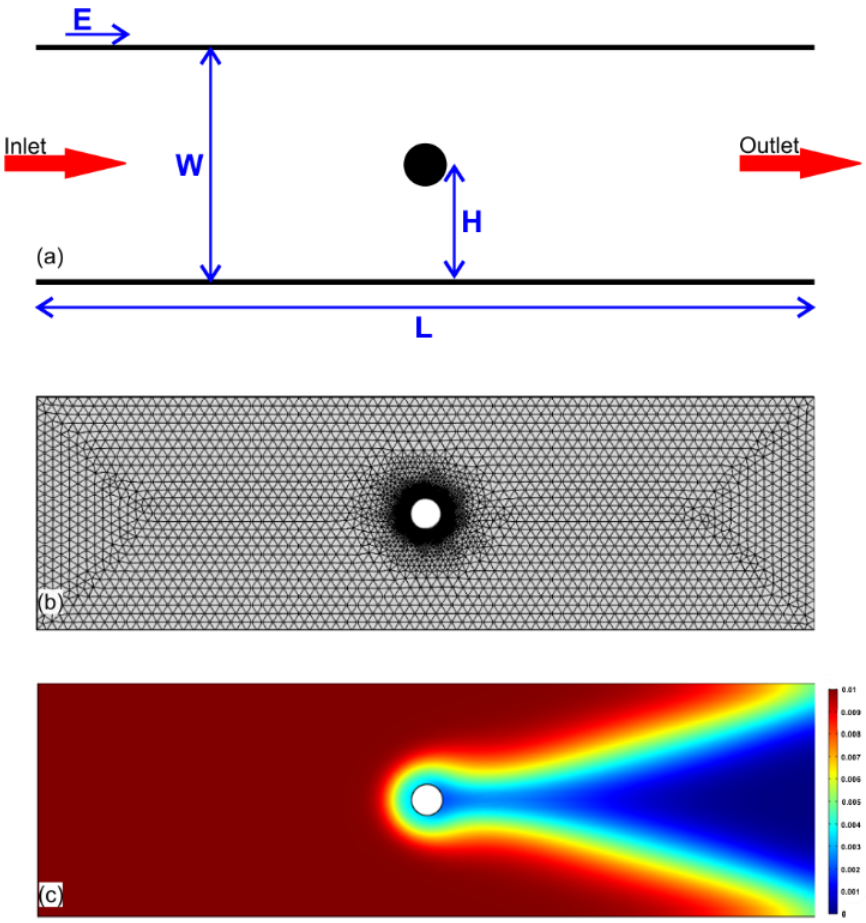

Figure 1: (a) Proposed design of the microfluidic system with the length of L=1000μm, the width of W=300μm, the distance between the lower boundary and the microfluidic channel H=150μm. While the inlet is the left boundary of the microchannel, the right boundary is the outlet. Left boundary and right boundary are also positive electrode and ground; thus, an electrical field is generated from left to right. (b) A mesh is applied to the solving domain because the simulation software employs FEA method. Denser mesh is required around of adsorbent microparticle surface, where the adsorption-desorption reaction occurs. (c) Adsorbate species are diluted in the flowing fluid with a certain concentration and fed to the inlet's microfluidic domain, and collected from the outlet.

3. Results and Discussion

An independent adsorption simulation is performed according to the conditions of the experimental study of Shirahama et al. [40] for validating the proposed numerical code. Adsorbate concentrations are compared for specific time values, as graphically displayed in Figure 2. Approximately a correlation of 98% is calculated between the numerical and the experimental values. Moreover, Eq. (8) is solved for determining the equilibrium surface adsorbate concentration, and exactly overlapping results are obtained from the proposed numerical code, which is $C_C^e q = 9.94x10^{-11} mol/m^2$. It can be concluded that adsorption modelling can be safely conducted with the proposed code.

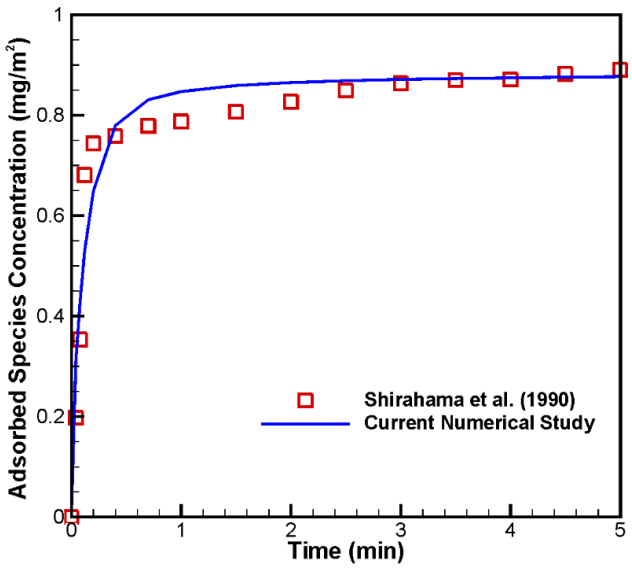

Figure 2: Results of the experimental data of Shirahama et al. (1990) are consistent with the results of the numerical code under the same conditions

Figure 3(a) indicates the time-dependent adsorbate concentration under varying external electrical field strengths. The general trend of adsorbent concentration is remaining at zero values for the initial times, dramatically increases when the adsorbate and adsorbent contacts, and then reaches the steady-state, where the rates of adsorption and desorption are equal. When the electrical field strength is increased, adsorbate concentration on the adsorbate surface also increases for a given time. Therefore, complete adsorption time is reached sooner for the relatively high electrical field strengths, as seen in Figure 3(b). 445.1 s – 270.6 s – 212.8 s – 183.3 s – 163.9 s of complete adsorption times are obtained for the electrical fields of E=100V/m – 200V/m – 300V/m – 400V/m – 500V/m, respectively. This acceleration is attenuated while the electrical field strength increases. Electrical field strength is directly related to the fluid flow velocity, which is also directly related to the diluted species' convective flux; thus, the adsorbate interacts with the adsor-

bent material quicker and longer. Similar findings are observed in the study of Hu et al. [41].

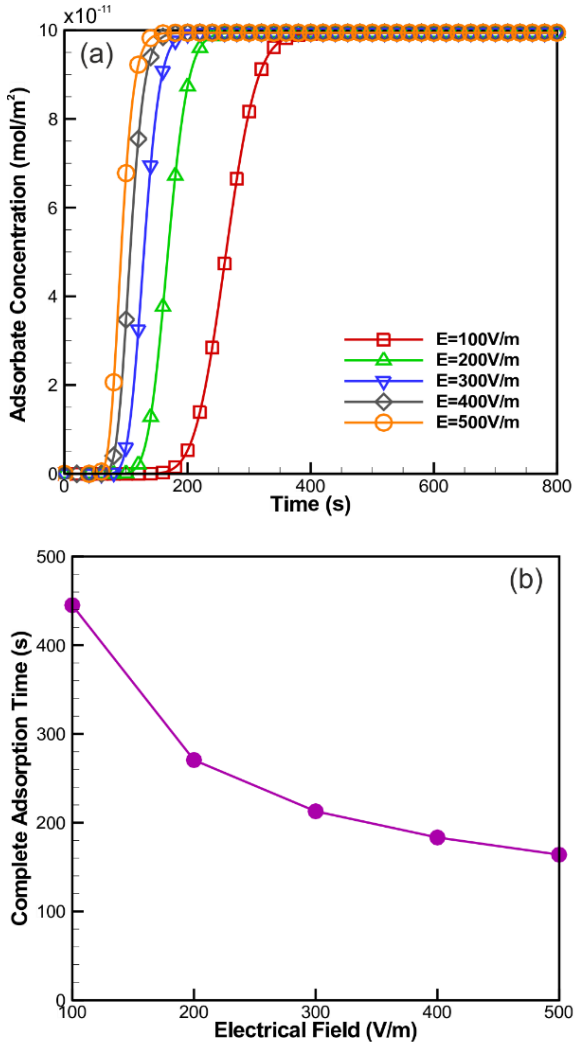

Figure 3: (a) Concentration of adsorbate species upon the adsorbent surface increases more rapidly when the relatively higher electrical field strength is applied. (b) Complete adsorption time is reached sooner with a relatively higher electrical field strength.

The time-dependent adsorption performance of the varying diameters of spherical microparticles is graphically displayed in Figure 4. The electrical field is selected for the most rapid complete adsorption time, which is $E = 500V/m$. As seen in Figure 4(a), when the microparticle diameter is increased, total adsorption time is reached at higher time values. The complete adsorption time for the diameters of $D_P = 20\mu m$ – 30μm – 40μm – 50μm – 60μm is 140.2s – 151.9s –

163.9s – 176.9s – 189.6s, respectively, which can be seen graphically in Figure 4(b). When the microparticle diameter is increased, more adsorbent sites occur upon the surface of the adsorbent. Therefore, complete adsorption time is reached for later times. Moreover, this increment is almost perfectly linear for the complete adsorption time, which the value of $R^2 = 0.9995$.

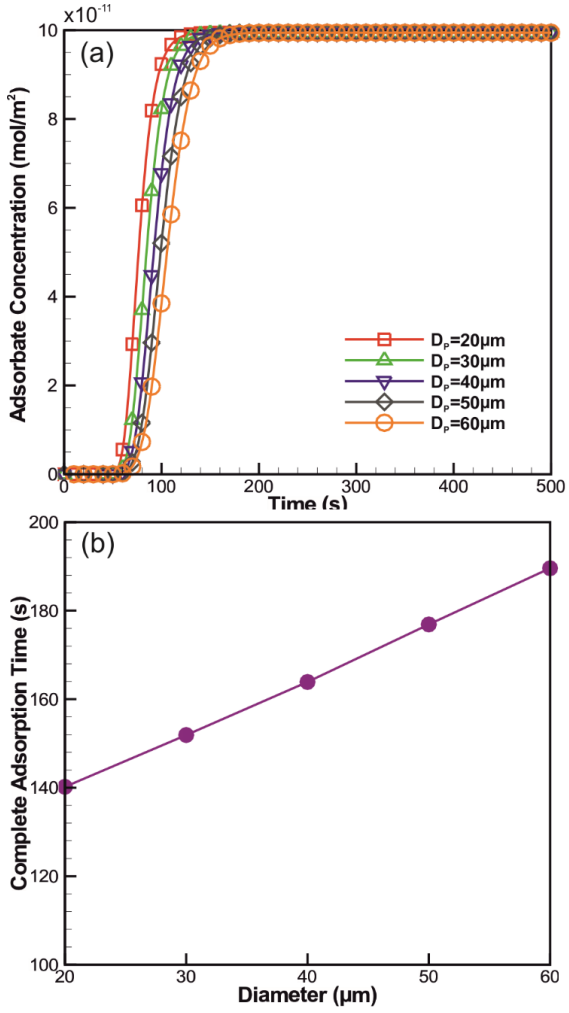

Figure 4: (a) Higher concentrations are obtained with relatively lower diameters at instant times. (b) Complete adsorption time is reached sooner with a relatively lower diameter

The influence of initial adsorbate concentration over the adsorption behavior is displayed in Figure 5. While the previous results are obtained for $C_{init} = 0.01 mol/m^3$, the values of $C_{init} = 0.05 mol/m^3$, $C_{init} = 0.15 mol/m^3$, $C_{init} = 0.2 mol/m^3$ are investigated along with the aforementioned value. As shown in Figure 5(a), a time-dependent increase in the adsorbate concentration is more rapid

for the relatively high initial adsorbate concentrations. This finding can be explained by enabling denser interaction between the adsorbate and the adsorbent. Complete adsorption times for the initial concentration values are determined as 203.8 s, 140.2 s, 118.5 s, 107.5 s, from the lowest initial concentration to the highest initial concentration, respectively, which is shown in Figure 5(b).

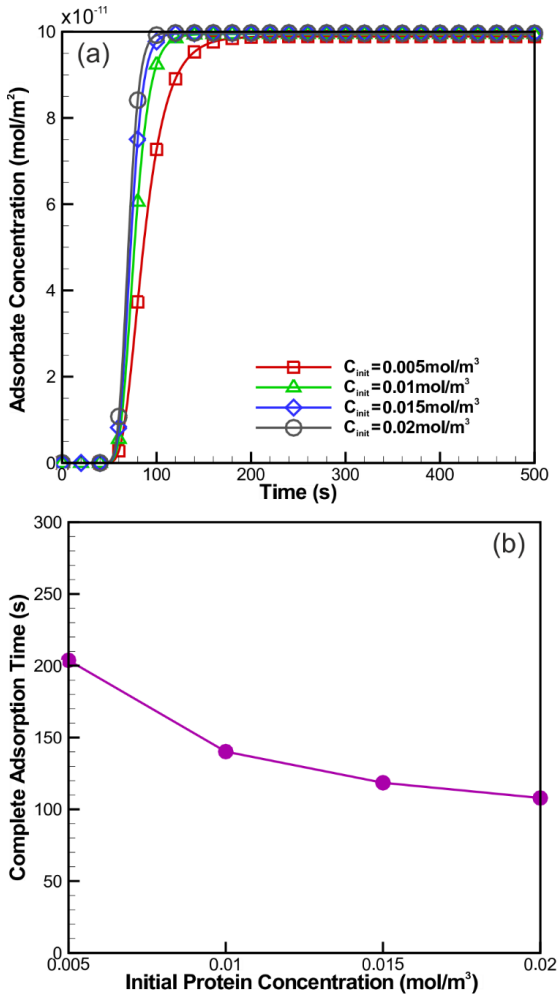

Figure 5: (a) Higher concentrations are obtained with relatively higher initial adsorbate concentration at instant times. (b) Complete adsorption time is reached sooner with a relatively higher initial adsorbate concentration

The adsorbent surface is relocated in the close proximity of a solid boundary, whether investigating the adsorption performance is influenced. By this means, the distance between the spherical adsorbate microparticle and the lower boundary of the microchannel is diminished to a few micrometers, i.e., H=10μm. During the investigation, the lower boundary remains non-functional. As illustrated in Fig-

ure 6, a slight increase is observed when the microparticle and the lower boundary are located in close proximity. The complete adsorption times for the usual formation and the close proximity formation are determined as 114 s and 140.2 s, respectively. It is previously proven that the complete adsorption time decreases with higher convective flux values. For the close proximity configuration, relatively larger convective flux is observed in the vicinity of the lower quadrant of the spherical microparticle due to the significantly decreased cross-section area of the flowing microchannel. This difference can be considered as the reason behind the observed slight difference between the resulting complete adsorption times.

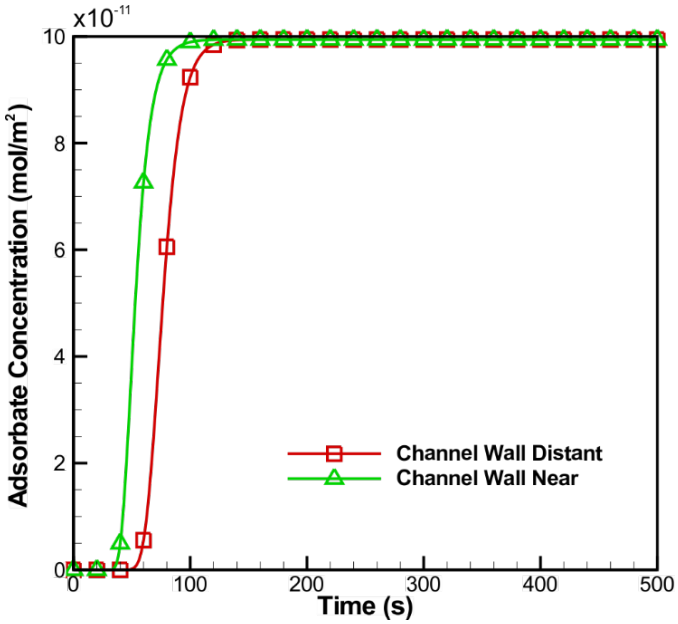

Figure 6: Adsorbed concentrations of diluted species are reached higher values sooner for a solid boundary near the adsorbent surface compared to the actual contrary situation.

The final investigation is based on the shape of the adsorbent surface; thus, triangular, rhombic, and square shapes are employed, along with the usual spherical geometry. Every geometry is placed to the center of the microchannel from their mass centers, and surface areas are held equal for better comparison. As shown in Figure 7, time-dependent variations in the adsorbent concentrations of the different geometries are nearly equal. Nevertheless, the most rapid adsorption is observed for triangular geometry, which equals 133.1 s. Spherical, rhombic, and square geometries are sorted as the second, the third, and the fourth with the complete adsorption times of 140.2 s, 143 s, 143.9 s, respectively.

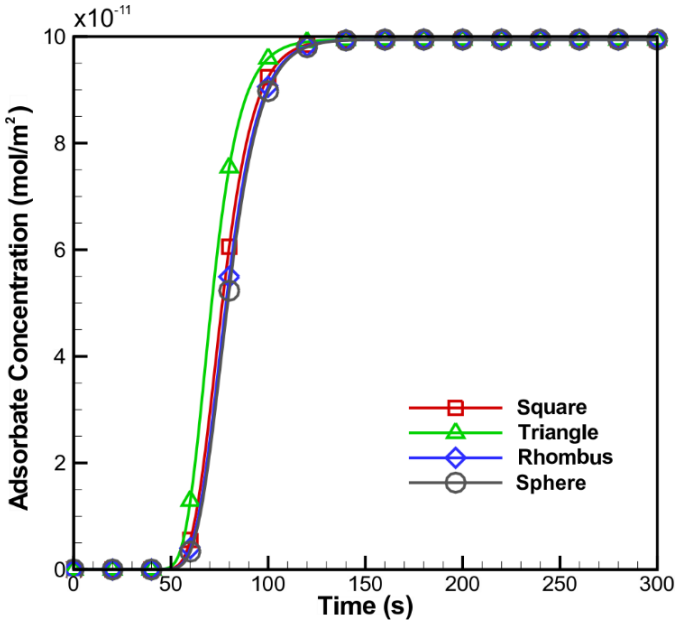

Figure 7: More rapid adsorption behavior is observed with the triangular-shaped adsorbent surface as compared to the entire spherical-shaped adsorbent surface. On the contrary, slower adsorption behavior is exhibited by the rhombic shaped and square-shaped adsorbent surfaces, respectively

4. Conclusions

In the present study, protein adsorption behavior upon a spherical solid surface, which is suspended within a microfluidic channel, is numerically investigated. The investigation is carried out by systematically varying the operational parameters of external electric field strength (E), particle diameter (D_P), the distance between the adsorbent surface and the lower boundary of the microchannel (H), and the geometrical shape of the adsorbent surface. Albumin is selected as the adsorbate material, and the adsorption-desorption phenomenon is modeled with the classical Langmuir model under a coarse-grained approach. Outcomes of the present study are listed below, which can be valid for the many protein species due to owning analogical nature.

1. The adsorbate concentration remains nearly zero at first, dramatically increases then, and reaches steady-state at the final.

2. The external electrical field's strength is directly proportional to the protein adsorption behavior due to providing quicker and longer interaction between the adsorbate and the adsorbent.

3. When the diameter of the spherical microparticle is increased, complete protein adsorption time decelerates due to relatively increased adsorption site concentrations for the larger surface areas.

Funding

This work is supported by Cukurova University Scientific Research Office financially under contract no FBA-2017-7960.

Competing interests

The authors declare that they have no conflict of interests.

Consent for publication

All authors read and approved the manuscript.

Rights and permissions

References

[1] Z. Adamczyk, "Modeling adsorption of colloids and proteins," *Current opinion in colloid & interface science*, vol. 17, no. 3, pp. 173–186, 2012.

[2] K. Nakanishi, T. Sakiyama, and K. Imamura, "On the adsorption of proteins on solid surfaces, a common but very complicated phenomenon," *Journal of bioscience and bioengineering*, vol. 91, no. 3, pp. 233–244, 2001.

[3] J. Buijs, W. T. James, W. Norde, J. Lyklema, *et al.*, "Adsorption of monoclonal iggs and their f (ab') 2 fragments onto polymeric surfaces," *Colloids and Surfaces B: Biointerfaces*, vol. 5, no. 1-2, pp. 11–23, 1995.

[4] I. Firkowska-Boden, X. Zhang, and K. D. Jandt, "Controlling protein adsorption through nanostructured polymeric surfaces," *Advanced healthcare materials*, vol. 7, no. 1, p. 1700995, 2018.

[5] A. C. Weiss, K. Krüger, Q. A. Besford, M. Schlenk, K. Kempe, S. Förster, and F. Caruso, "In situ characterization of protein corona formation on silica microparticles using confocal laser scanning microscopy combined with microfluidics," *ACS applied materials & interfaces*, vol. 11, no. 2, pp. 2459–2469, 2019.

[6] L. Shang and G. U. Nienhaus, "In situ characterization of protein adsorption onto nanoparticles by fluorescence correlation spectroscopy," *Accounts of chemical research*, vol. 50, no. 2, pp. 387–395, 2017.

[7] R. M. Visalakshan, M. N. MacGregor, S. Sasidharan, A. Ghazaryan, A. M. Mierczynska-Vasilev, S. Morsbach, V. Mailänder, K. Landfester, J. D. Hayball, and K. Vasilev, "Biomaterial surface hydrophobicity-mediated serum protein adsorption and immune responses," *ACS applied materials & interfaces*, vol. 11, no. 31, pp. 27615–27623, 2019.

[8] Z. Wang, Y. Yan, and L. Qiao, "Protein adsorption on implant metals with various deformed surfaces," *Colloids and Surfaces B: Biointerfaces*, vol. 156, pp. 62–70, 2017.

[9] A. Hasan, S. K. Pattanayek, and L. M. Pandey, "Effect of functional groups of self-assembled monolayers on protein adsorption and initial cell adhesion," *ACS Biomaterials Science & Engineering*, vol. 4, no. 9, pp. 3224–3233, 2018.

[10] A. Manz, D. J. Harrison, E. M. Verpoorte, J. C. Fettinger, A. Paulus, H. Lüdi, and H. M. Widmer, "Planar chips technology for miniaturization and integration of separation techniques into monitoring systems: capillary electrophoresis on a chip," *Journal of Chromatography A*, vol. 593, no. 1-2, pp. 253–258, 1992.

[11] G. M. Whitesides, "The origins and the future of microfluidics," *nature*, vol. 442, no. 7101, pp. 368–373, 2006.

[12] J. Mairhofer, K. Roppert, and P. Ertl, "Microfluidic systems for pathogen sensing: a review," *Sensors*, vol. 9, no. 6, pp. 4804–4823, 2009.

[13] A. M. Foudeh, T. F. Didar, T. Veres, and M. Tabrizian, "Microfluidic designs and techniques using lab-on-a-chip devices for pathogen detection for point-of-care diagnostics," *Lab on a Chip*, vol. 12, no. 18, pp. 3249–3266, 2012.

[14] B. Nasseri, N. Soleimani, N. Rabiee, A. Kalbasi, M. Karimi, and M. R. Hamblin, "Point-of-care microfluidic devices for pathogen detection," *Biosensors and Bioelectronics*, vol. 117, pp. 112–128, 2018.

[15] J. Kim, I. Hwang, D. Britain, T. D. Chung, Y. Sun, and D.-H. Kim, "Microfluidic approaches for gene delivery and gene therapy," *Lab on a Chip*, vol. 11, no. 23, pp. 3941–3948, 2011.

[16] M. A. Tomeh and X. Zhao, "Recent advances in microfluidics for the preparation of drug and gene delivery systems," *Molecular Pharmaceutics*, vol. 17, no. 12, pp. 4421–4434, 2020.

[17] R. Riahi, A. Tamayol, S. A. M. Shaegh, A. M. Ghaemmaghami, M. R. Dokmeci, and A. Khademhosseini, "Microfluidics for advanced drug delivery systems," *Current Opinion in Chemical Engineering*, vol. 7, pp. 101–112, 2015.

[18] S. Damiati, U. B. Kompella, S. A. Damiati, and R. Kodzius, "Microfluidic devices for drug delivery systems and drug screening," *Genes*, vol. 9, no. 2, p. 103, 2018.

[19] J. Ahn, J. Ko, S. Lee, J. Yu, Y. Kim, and N. L. Jeon, "Microfluidics in nanoparticle drug delivery; from synthesis to pre-clinical screening," *Advanced drug delivery reviews*, vol. 128, pp. 29–53, 2018.

[20] N. W. Choi, M. Cabodi, B. Held, J. P. Gleghorn, L. J. Bonassar, and A. D. Stroock, "Microfluidic scaffolds for tissue engineering," *Nature materials*, vol. 6, no. 11, pp. 908–915, 2007.

[21] Y. Jun, E. Kang, S. Chae, and S.-H. Lee, "Microfluidic spinning of micro- and nano-scale fibers for tissue engineering," *Lab on a Chip*, vol. 14, no. 13, pp. 2145–2160, 2014.

[22] Q. Smith and S. Gerecht, "Going with the flow: microfluidic platforms in vascular tissue engineering," *Current opinion in chemical engineering*, vol. 3, pp. 42–50, 2014.

[23] R. Wu and T. Kim, "Review of microfluidic approaches for fabricating intelligent fiber devices: importance of shape characteristics," *Lab on a Chip*, vol. 21, no. 7, pp. 1217–1240, 2021.

[24] W. Li, L. Zhang, X. Ge, B. Xu, W. Zhang, L. Qu, C.-H. Choi, J. Xu, A. Zhang, H. Lee, *et al.*, "Microfluidic fabrication of microparticles for biomedical applications," *Chemical Society Reviews*, vol. 47, no. 15, pp. 5646–5683, 2018.

[25] B. Wang, P. Prinsen, H. Wang, Z. Bai, H. Wang, R. Luque, and J. Xuan, "Macroporous materials: microfluidic fabrication, functionalization and applications," *Chemical Society Reviews*, vol. 46, no. 3, pp. 855–914, 2017.

[26] X. Weng and S. Neethirajan, "Ensuring food safety: Quality monitoring using microfluidics," *Trends in food science & technology*, vol. 65, pp. 10–22, 2017.

[27] H. Gao, C. Yan, W. Wu, and J. Li, "Application of microfluidic chip technology in food safety sensing," *Sensors*, vol. 20, no. 6, p. 1792, 2020.

[28] S. Choi and J. Chae, "A microfluidic biosensor based on competitive protein adsorption for thyroglobulin detection," *Biosensors and Bioelectronics*, vol. 25, no. 1, pp. 118–123, 2009.

[29] K. Tsougeni, P. S. Petrou, D. P. Papageorgiou, S. E. Kakabakos, A. Tserepi, and E. Gogolides, "Controlled protein adsorption on microfluidic channels with engineered roughness and wettability," *Sensors and Actuators B: Chemical*, vol. 161, no. 1, pp. 216–222, 2012.

[30] Y. Xu, M. Takai, T. Konno, and K. Ishihara, "Coating of anionic phospholipid polymer onto silica-based microchannel to minimize nonspecific protein adsorption," in *Key Engineering Materials*, vol. 342, pp. 797–800, Trans Tech Publ, 2007.

[31] G. W. Greene, E. Duffy, A. Shallan, A. Wuethrich, and B. Paull, "Electrokinetic properties of lubricin antiadhesive coatings in microfluidic systems," *Langmuir*, vol. 32, no. 7, pp. 1899–1908, 2016.

[32] D. Mark, S. Haeberle, G. Roth, F. Von Stetten, and R. Zengerle, "Microfluidic lab-on-a-chip platforms: requirements, characteristics and applications," *Microfluidics based microsystems*, pp. 305–376, 2010.

[33] J. H. Masliyah and S. Bhattacharjee, *Electrokinetic and colloid transport phenomena*. John Wiley & Sons, 2006.

[34] X. Quan, J. Liu, and J. Zhou, "Multiscale modeling and simulations of protein adsorption: progresses and perspectives," *Current Opinion in Colloid & Interface Science*, vol. 41, pp. 74–85, 2019.

[35] R. A. Latour, "Molecular simulation of protein-surface interactions: Benefits, problems, solutions, and future directions," *Biointerphases*, vol. 3, no. 3, pp. FC2–FC12, 2008.

[36] M. Pernemalm, A. Sandberg, Y. Zhu, J. Boekel, D. Tamburro, J. M. Schwenk, A. Björk, M. Wahren-Herlenius, H. Åmark, C.-G. Östenson, *et al.*, "In-depth human plasma proteome analysis captures tissue proteins and transfer of protein variants across the placenta," *Elife*, vol. 8, p. e41608, 2019.

[37] Z. Adamczyk, "Particles at interfaces: Interactions, deposition," *Structure*, vol. 9, p. 1, 2006.

[38] R. A. Latour, "The langmuir isotherm: a commonly applied but misleading approach for the analysis of protein adsorption behavior," *Journal of Biomedical Materials Research Part A*, vol. 103, no. 3, pp. 949–958, 2015.

[39] K. Baler, O. A. Martin, M. A. Carignano, G. Ameer, J. A. Vila, and I. Szleifer, "Electrostatic unfolding and interactions of albumin driven by ph changes: a molecular dynamics study," *The journal of physical chemistry B*, vol. 118, no. 4, pp. 921–930, 2014.

[40] H. Shirahama, J. Lyklema, and W. Norde, "Comparative protein adsorption in model systems," *Journal of colloid and interface science*, vol. 139, no. 1, pp. 177–187, 1990.

[41] G. Hu, Y. Gao, and D. Li, "Modeling micropatterned antigen–antibody binding kinetics in a microfluidic chip," *Biosensors and Bioelectronics*, vol. 22, no. 7, pp. 1403–1409, 2007.